Characterization of semiconductors from photoconductivity techniques: Photocarrier grating techniques

Christophe Longeaud, Javier Schmidt, Jean-Paul Kleider

4

Characterization of semiconductors from photoconductivity techniques: Photocarrier grating techniques

Christophe Longeaud[1], Javier Schmidt[2] and Jean-Paul Kleider[1]

[1] Group of Electrical Engineering – Paris (GeePs), CNRS, CentraleSupelec, Université Paris-Saclay, Sorbonne Université, 11 rue Joliot Curie, 91190 Gif sur Yvette, France

[2] Instituto de Física del Litoral (IFIS–Litoral), CONICET-UNL, Güemes 3450, S3000GNL Santa Fe, Argentina

Abstract

In this chapter we detail photoconductivity techniques based on the illumination of a sample in a coplanar electrode configuration with a light intensity periodically modulated in space. Such a modulation is obtained from the interferences of two laser beams that illuminate the space between the electrodes. This illumination can be constant in time as in the steady-state photocarrier grating (SSPG) proposed by D. Ritter *et al.*, modulated in time as in the modulated photocarrier grating (MPG) detailed by K. Hattori *et al.*, moving at a constant speed perpendicularly to the electrodes in the moving grating technique (MGT) imagined by U. Haken *et al.*, or oscillating perpendicularly to the electrodes as in the oscillating photocarrier grating (OPG) technique developed by F. Ventosinos *et al.*. All these experiments are practically and theoretically detailed. For each of them we present the experimental set-up and the theoretical background from which transport parameters, such as the ambipolar diffusion length, can be extracted. We also show that, under some assumptions, information on the lifetimes and density of states (DOS) can be obtained, and, for some of them, a DOS spectroscopy can be achieved if the experiments are performed at various temperatures and/or generation rates. It is also shown that some of these techniques are complementary to other techniques, like the steady-state photoconductivity (SSPC) or the modulated photocurrent (MPC) experiments, the combination of these techniques bringing information that could not be obtained from a single one. All these techniques and their expected results are illustrated by means of numerical calculations as well as some experimental results.

Keywords : photoconductivity, photocarrier grating, ambipolar diffusion length, lifetime, density of states

4.1. Introduction

The basic principle of the techniques described in this chapter is to illuminate the part of a sample located in the gap between two parallel coplanar electrodes with an interfering light having an adjustable grating spacing. These interferences are obtained by the superimposition of two coherent laser beams polarized in the direction parallel to the electrodes. The angle θ between the beams fixes the grating spacing Λ. One of these beams has always an intensity much lower, by a factor 10 to 50, than the other one that will be called the main beam. This main beam sets the steady state of the film while the other one, that we shall call the probe beam, induces a small perturbation to this steady state. From the response of the sample to this perturbation one can extract information on the transport properties of the material, bearing in mind that the experimental conditions to extract this information vary from one experiment to the other. Thus, the parameters deduced from this response may vary from one experiment to the other.

In the steady-state photocarrier grating (SSPG) technique one measures the excess of photocurrent generated by the probe beam when the sample is biased with a low DC voltage applied between the electrodes. These measurements are performed both when the two beams interfere and when the interference pattern is suppressed by changing the polarization of the light of one of the beams [1]. The information is essentially contained in the ratio of the two photocurrents and its dependence on the grating period.

A way to introduce a temporal component to the SSPG technique was proposed by K. Hattori *et al.* [2]. For this purpose, they proposed to investigate on transport properties of thin films by introducing a time modulation of the grating at an adjustable frequency, and to study the evolution of the excess photocurrent at different frequencies and different grating periods. The position of the interferences being constant, a small voltage bias has to be set between the sample electrodes to generate this photocurrent. This experiment is called the modulated photocarrier grating (MPG) technique. Combined with the modulated photocurrent (MPC) experiment, one can deduce information on the regime under which the sample is working, lifetime regime or relaxation time regime, and correct the diffusion length measured by SSPG. Later on, it was proposed by J. A. Schmidt *et al.* to combine MPC and MPG to perform a density of states (DOS) spectroscopy of the material under investigation [3].

The moving grating technique (MGT) was imagined by Haken, Hundhausen and Ley also to introduce a temporal component to the SSPG. This temporal component is obtained by shifting the frequency ν of the light of each beam, and this shift generates a grating moving at a velocity v_{gr} linked to the frequency difference $\Delta\nu$ between the beams. This movement of the grating gives rise to a steady current density J_{sc}, even without any voltage bias applied, whose intensity depends on v_{gr} [4, 5]. Materials parameters can be extracted from a fit of a plot of J_{sc} versus v_{gr} for different fluxes or different grating periods.

Finally, an alternating version of the MGT was proposed by F. Ventosinos and coworkers to study the excess of photocurrent created by the oscillation of the interference pattern in between the electrodes [6]. This method was called the oscillating photocarrier grating (OPG), and aimed at the study of the variations of the excess photocurrent with the frequency of the oscillations. As in the case of MGT, an excess photocurrent can be obtained even without the application of a voltage bias between the electrodes. It was shown that a density of states spectroscopy can be achieved from the results of this experiment.

Similar techniques, based on photocarrier gratings, were developed in another field of research, namely to study photorefractive crystals. For a review see [7].

For all the techniques exposed here, a complete analysis of the processes involved in the material under investigation can be performed taking account of distributions of monovalent states of both donor type, $N^{DON}(E)$, and acceptor type, $N^{ACC}(E)$, starting from the usual continuity equations,

where all the quantities are supposed to depend spatially only on x, measured on an axis perpendicular to the electrodes

$$\frac{\partial n(x,t)}{\partial t} = G(x,t) - R_{\mathrm{n}}(x,t) + \frac{1}{q}\frac{\partial}{\partial x}[J_{\mathrm{n}}(x,t)] \quad , \qquad (4.1)$$

$$\frac{\partial p(x,t)}{\partial t} = G(x,t) - R_{\mathrm{p}}(x,t) - \frac{1}{q}\frac{\partial}{\partial x}[J_{\mathrm{p}}(x,t)] \quad , \qquad (4.2)$$

and Poisson's equation, relating the electric field $\xi(x, t)$ to the local charge densities

$$\frac{d\xi(x,t)}{dx} = \frac{q}{\varepsilon\varepsilon_0}\left[p(x,t) + \int_{E_{\mathrm{V}}}^{E_{\mathrm{C}}}[1 - f(E,x,t)]N^{\mathrm{DON}}(E)dE - n(x,t) - \int_{E_{\mathrm{V}}}^{E_{\mathrm{C}}} f(E,x,t)N^{\mathrm{ACC}}(E)dE\right] . \qquad (4.3)$$

In these equations q is the absolute value of the electron charge, ε and ε_0 are the relative permittivity of the material and the vacuum permittivity, respectively, E is the energy, E_{C} (E_{V}) the energy at the bottom (top) of the conduction (valence) band, $f(E, x, t)$ the occupation function of the gap states, n (p) the free electron (hole) concentration, $G(x, t)$ the generation rate at a position x, $R_{\mathrm{n}}(x, t)$ ($R_{\mathrm{p}}(x, t)$) the recombination rate for electrons (holes), and $J_{\mathrm{n}}(x, t)$ ($J_{\mathrm{p}}(x, t)$) the electron (hole) current density.

In the case of SSPG, the time component can be suppressed and Eqs. (4.1) and (4.2) can be simplified into

$$G(x) - R_{\mathrm{n}}(x) = -\mu_{\mathrm{n}}\frac{d}{dx}[n(x)\xi(x)] - D_{\mathrm{n}}\frac{d^2n(x)}{dx^2} \quad , \qquad (4.4)$$

$$G(x) - R_{\mathrm{p}}(x) = \mu_{\mathrm{p}}\frac{d}{dx}[p(x)\xi(x)] - D_{\mathrm{p}}\frac{d^2p(x)}{dx^2} \quad , \qquad (4.5)$$

where μ_{n} (μ_{p}) is the extended-states mobility and D_{n} (D_{p}) the diffusion coefficient for electrons (holes).

In the following we shall briefly detail all the techniques presented above and show that for some of them it is possible to deduce the density of states of the material from a solution of the above equations.

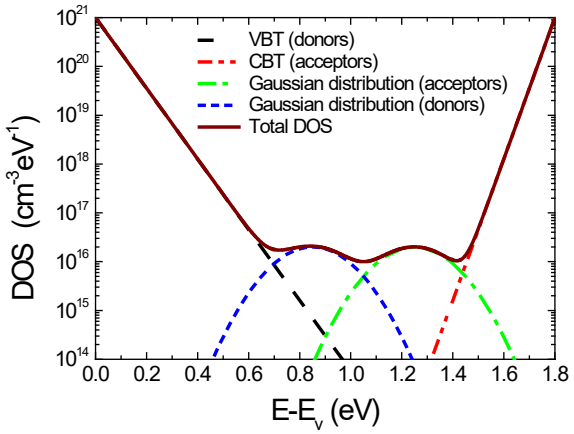

Figure 4.1. Typical DOS for a-Si:H used in our simulations. It consists of the sum of two exponential band tail distributions, the donor-type valence band tail (VBT) and the acceptor-type conduction band tail (CBT), and two deep Gaussian distributions of donor- and acceptor-type that represent the dangling bond defects. These have the same maximum and full width at half maximum values and are shifted by 0.4 eV.

In addition, to underline some of the theoretical calculations presented here and to show their applicability, we have performed many numerical calculations. Though all the techniques presented here can be applied to several types of materials, we have essentially illustrated these numerical calculations applying them to hydrogenated amorphous silicon (a-Si:H), for most of our studies have

been applied to this material. In Fig. 4.1 we present a typical DOS of this material, made of two exponentially varying band tail state distributions, a valence band tail (VBT) of donor states and a conduction band tail (CBT) of acceptor states, and two Gaussian-shaped deep defect distributions, as acceptor and donor states distributions. In our numerical calculations it is possible to modify the characteristic parameters of these distributions, as well as to choose the 'experimental' conditions (Flux, temperature, type of experiment, …) and the transport parameters (band gap, mobilities, capture coefficients for each of the distributions, …) to calculate the data that one would obtain from a given characterization technique. These results can eventually be a help to check for the experimental applicability of the theoretical developments and to define the proper experimental conditions under which the characterizations must be done.

4.2. Steady-state photocarrier grating (SSPG)

4.2.1. Fundamentals

The steady state photocarrier grating technique was proposed in 1986 by D. Ritter *et al.* [1] to investigate the ambipolar diffusion length L_{amb} of photoconductive semi-insulating materials such as a-Si:H and GaAs, among others [8]. The basic principle of this technique is to illuminate with two laser beams, interfering or not, the gap between two parallel and preferably ohmic electrodes deposited on a photoconductive sample (though D. Ritter claimed that the contacts need not be ohmic, since only small changes in the photocurrent are measured). The occurrence of interferences depends on the light polarization of the beams. If the polarization of both light beams is parallel to the electrodes an interference pattern is formed on and in the sample, the grating period Λ being a function of the wavelength λ and of the angle θ between the beams (see Fig. 4.2)

$$\Lambda = \frac{\lambda}{2\sin(\theta/2)} \quad . \qquad (4.6)$$

At a coordinate x on an axis perpendicular to the electrodes, taking its origin on one of them, the light intensity $I(x)$ can be written

$$I(x) = I_1 + I_2 + 2\gamma_0\sqrt{I_1 I_2}\cos\left(\frac{2\pi x}{\Lambda}\right) \quad , \qquad (4.7)$$

where I_1 and I_2 are the intensities of each beam and γ_0 is a factor between zero and unity taking account of the quality of the interferences (*e.g.*, the contrast). If the polarizations of the beams are crossed interferences disappear ($\gamma_0 = 0$) and the total intensity impinging the sample is constant and equal to the superimposition of the intensities of each beam, $I(x) = I_1 + I_2$.

A schematic diagram of an SSPG setup is presented in Fig. 4.2. The light emitted from a He-Ne laser ($\lambda = 632.8$ nm), the polarization of which is perpendicular to the plane of the figure, is split in two beams with a beam splitter (BS). On one of the beam paths, a $\lambda/2$ plate can be added to rotate the light polarization by 90° suppressing the formation of the interferences. This beam, of intensity I_1, will be called the main beam in the following. On the path of the other beam, called the probe beam in the following, is placed a neutral density (ND) filter, to attenuate its intensity to a value I_2, and a chopper to vary periodically I_2 with time. The intensity of the probe beam is attenuated, so that its action can be considered as a small perturbation of the main beam that sets the steady-state of the film. Subsequently, these beams are directed by different mirrors toward the sample, making an angle θ between them ($\theta/2$ with the normal to the sample surface). The sample is biased with a small DC voltage and one measures the excess of current resulting from the superimposition of the probe beam to the main beam. To measure accurately this excess of current, the probe beam is chopped at a low

frequency, say 10 Hz, and, after amplification of this current by a current-voltage converter, its amplitude is recorded by means of a lock-in amplifier synchronized with the chopper.

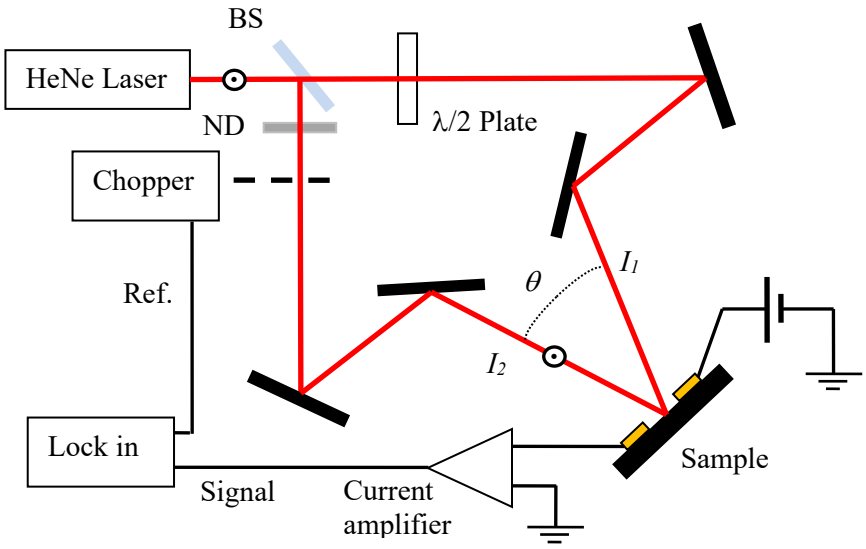

Figure 4.2. Schematic diagram of a 'standard' SSPG bench.

Fixing the position of the $\lambda/2$ plate, so that the polarizations of the two beams are parallel to the electrodes, generates interferences in the sample and an excess of current, I_{wi}, can be recorded. If the $\lambda/2$ plate is rotated, so that the polarizations of the beams are crossed, the two beams are simply superimposing, and one measures an excess of current I_{woi}. Ritter and coworkers have shown that the quantity $\beta = I_{wi}/I_{woi}$ could be written as a function of the ambipolar diffusion length of the carriers, L_{amb}, as

$$\beta(\Lambda) = 1 - \frac{2\gamma\gamma_0^2}{\left[1+\left(\frac{2\pi L_{amb}}{\Lambda}\right)^2\right]^2} \quad , \qquad (4.8)$$

where γ is defined as the logarithmic derivative of the photocurrent I_{ph} with respect to the steady and uniform generation rate, G_0,

$$\gamma = \frac{\partial \ln(I_{ph})}{\partial \ln(G_0)} \quad . \qquad (4.9)$$

By measuring I_{wi} and I_{woi} for several values of θ, and thus for several values of the grating period Λ, the diffusion length can be obtained from a fit of the $\beta(\Lambda)$ curve.

Another method to extract L_{amb} from the SSPG data is to modify Eq. (4.8) to end with

$$\left(\frac{2\pi}{\Lambda}\right)^2 = \left(\frac{1}{L_{amb}}\right)^2 \left[\frac{\sqrt{\gamma\gamma_0^2}}{\sqrt{(1-\beta(\Lambda))/2}} - 1\right] \quad , \qquad (4.10)$$

that leads to a linear variation of $(2\pi/\Lambda)^2$ with $1/\sqrt{(1-\beta(\Lambda))/2}$. This formula was proposed by I. Balberg *et al.* to underline the self-consistency of the SSPG technique [9]. The advantage of such a plot is that any deviation from a straight line is easily seen and, in this case, the accuracy of the extracted L_{amb} value can be questionable [10]. Another advantage is that the extrapolation of the curve defined by Eq. (4.10) toward the ordinate axis gives the value $-(1/L_{amb})^2$ from which the L_{amb} value can be deduced.

Illustrations for both methods are presented in Figs. 4.3a and 4.3b. In Fig. 4.3a, Eq. (4.8) is used to fit (red line) the SSPG data (red circles) obtained on a polymorphous hydrogenated silicon (pm-Si:H) sample, and in Fig. 4.3b the same data are plotted following Balberg's formula (blue circles) and fitted by a straight blue line using Eq. (4.10) to yield in both cases a diffusion length of 200 nm. Note that in Fig. 4.3b the straight line was extrapolated toward the ordinate axis giving a value of -25 μm^{-2} from which the value of L_{amb} = 0.2 µm can be deduced.

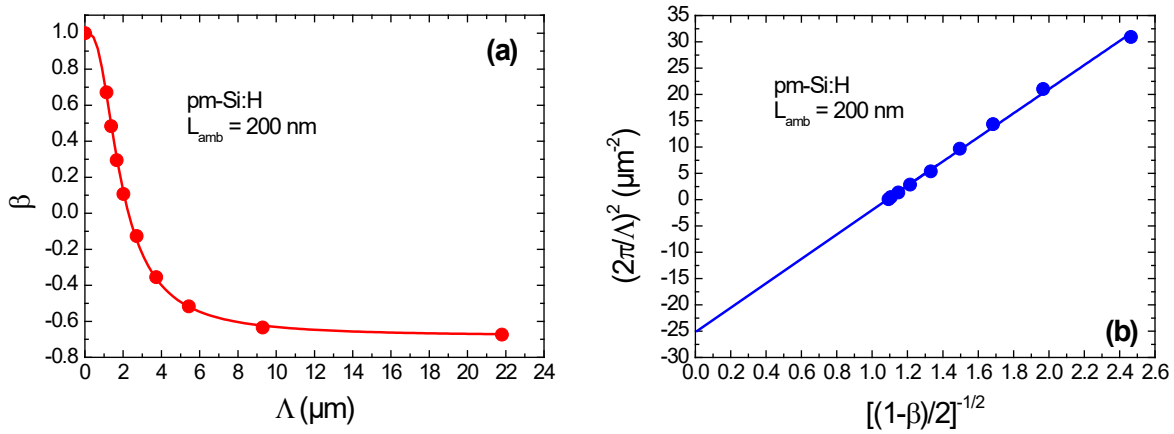

Figure 4.3. (a) SSPG data obtained on a pm-Si:H film (red circles) fitted with Eq. (4.8) (red line), and (b) plotted following Balberg's formula (Eq. (4.10), blue circles) and fitted with a straight blue line. Both fits yield the same value of 200 nm for the ambipolar diffusion length.

Since the pioneering work of Ritter *et al.*, many publications were dedicated to a thorough study of the SSPG technique. It is impossible to quote all of them and we shall present just a rapid overview in the following. Theoretical investigations were done on the spatial variations of the electron and hole densities under interferences illumination and the influence of the applied electric field [11, 12]. The influence of the dark conductivity [8, 10], of the dielectric relaxation time [11-15], of traps [16, 17] and of surface states [18] were investigated. Reviews of the SSPG technique and its application to several types of thin films were proposed by R. Brüggemann [19, 20].

The general trends coming out of these studies are that, to lead to reliable values of L_{amb}, the SSPG experiment must be ideally performed:

a/ In the lifetime regime, that is under conditions for which the carrier lifetime is much larger than the dielectric relaxation time τ_d,

b/ With a 'low' electric field applied in between the electrodes,

c/ With a 'low' frequency to measure with a lock-in amplifier the contribution of the probe beam to the excess current.

Under these conditions, the interferences impinging the sample create several arrays: arrays of free carriers and arrays of trapped carriers that eventually generate arrays of space charge and of internal electric field. If the grating period is small, these arrays are blurred and may even vanish under the influence of the diffusion of carriers. In that case, the excesses of current resulting from the addition of the probe beam to the main beam with or without interferences are almost equivalent, leading to a value of β close to one. On the other hand, with large grating periods a space charge array of minority carriers, resulting from the differences of the transport properties of the minority and majority carriers, establishes. The drift in between the electrodes of the majority carriers, under the influence of the applied field, is limited by the average internal field created by this space charge array. That is why the frequency of the chopper must be 'low', meaning that a quasi-steady-state is reached for the distribution of space charge. That is also why the applied field must be 'low', so that it does not excessively influence the space charge distribution, modifying the internal field distribution.

Of course, these two 'lows' ('low' frequency and 'low' field) are material dependent. For a-Si:H we expect that a field of the order of 100 V/cm and a frequency of the order of 10 Hz are convenient to perform reliable SSPG measurements.

An interesting point is that, in the SSPG technique, the limitation of the transport of the majority carriers by the minority carrier space charge is similar to the phenomenon of limitation of the majority carriers current by the space charge developed by the minority carriers in a device, if the latter are not extracted properly from the device. This point was confirmed from our long work on the study of a-Si:H thin films and devices, for which we found that it is useless to make a device with a thin film having a low L_{amb} value. On the other hand, if a device presents a weak energy conversion with an absorber presenting a large diffusion length, the reason may come from other issues such as bad interfaces, resistive contacts, … Such a behavior was also observed with organic thin films and devices, where the best devices were those incorporating films with the largest L_{amb} [21]. Therefore, as also underlined by I. Balberg [12], the SSPG technique seems to be an excellent technique to investigate transport properties of a material before incorporating it into a solar cell device.

However, the major drawback of this experiment in its first designs, for instance as in Fig. 4.2, is that the angle between the two beams has to be set manually for each value of Λ. Therefore, it was difficult to use it as a systematic characterization technique to study the influence of a deposition parameter on the quality of the prepared film, because of the amount of time needed to obtain a $\beta(\Lambda)$ curve. That is why we have designed an automated bench, capable of covering a large range of Λ values within a few minutes.

4.2.2. Description of an automated SSPG bench

This automated SSPG bench has been described in details in [22]. We recall here the basic ideas of this realization, a schematic drawing of which is presented in Fig. 4.4. As in the standard set up, a laser beam coming from a He-Ne laser, polarized perpendicularly to the plane of the figure, is split into two beams. One beam, the probe one, is chopped and attenuated whereas a $\lambda/2$ plate is set on the path of the other one, the main beam, to rotate the polarization of the light. The path of the main beam is chosen so that it reaches the sample between the electrodes and perpendicularly to its plane, while the path of the probe beam is a little bit more complicated. First, it is sent toward a mobile mirror fixed on a rail. This mirror can be moved along the rail so that the beam is reflected toward one of the return mirrors, the angle between the main beam and the probe beam, when they reach the film, depending on the chosen return mirror. The paths of both beams must be very close, so that their difference is much less than the coherence length of the laser beam. For this purpose the rail, on which the mobile mirror is moved, is not parallel to the main beam. In addition, just before the mobile mirror, two mirrors are added to adjust the total path of the probe beam within ± 1 cm of that of the main beam.

The positions of the return mirrors are chosen so that the grating period Λ varies in the range from ~ 1 µm, for the mirror the closest to the sample, to more than 20 µm for the mirror the farthest from the sample. Note that, because of the path geometry chosen for the beams to illuminate the sample, the grating period is not defined according to Eq. (4.6), but rather by $\Lambda = \lambda/\sin(\theta)$.

This system saves the time needed to correctly align manually the two beams before they reach the sample for each Λ, as it is the case in the standard bench. All the alignments for each return mirror are tuned once, and for further measurements on other samples the only adjustment is to fix the sample onto the sample holder. The position of the mobile mirror, the rotation of the $\lambda/2$ plate and the acquisition of the data are all computer controlled. The system achieves a complete measurement within 5 min.

Experimentally, we were able to measure ambipolar diffusion lengths of several types of materials such as a-Si:H, poly-c-Si, Sb_2S_3, organic semiconductors… Since the sample position is fixed it can be set into a cryostat, opening the possibility to study materials that have to be kept under vacuum, such as organic blends (*e.g.* P3HT-PCBM) and perovskites [21, 23]. Considering the range of Λ available with this bench, the diffusion lengths that can be investigated are in the range of 50 – 1500 nm. Hence, such a system can be used for routine characterization by laboratories and even by the photovoltaic thin film industry, on a large variety of materials.

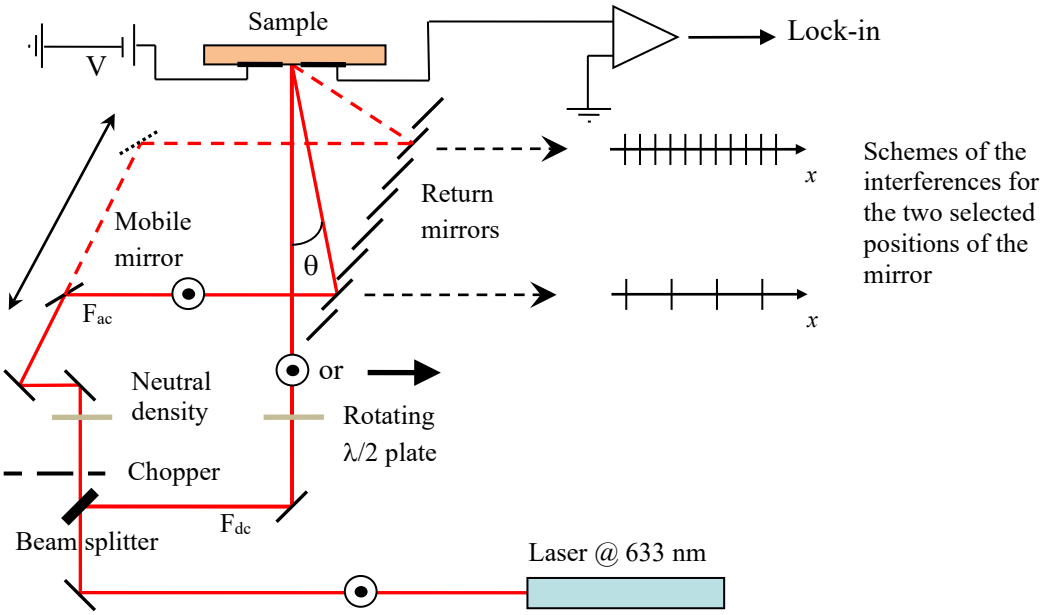

Figure 4.4. Schematic diagram of an improved SSPG bench enabling automated diffusion length measurement.

4.2.3. Use of the SSPG technique to derive the DOS

The non-uniform illumination given by Eq. (4.7) leads to a spatially modulated generation rate,

$$G(x) = G_0 + \Delta G\, cos(kx) \tag{4.11}$$

with $k = 2\pi/\Lambda$, $G_0 = G_1 + G_2$ and $\Delta G = 2\gamma_0\sqrt{G_1 G_2}$, G_1 and G_2 being the generation rates originating from I_1 and I_2, respectively. This spatially modulated generation rate in turn creates free electrons and holes distributions, $n(x)$ and $p(x)$, with the same period. However, since electrons and holes have different diffusion coefficients, the amplitudes and phases of the two distributions will differ, generating an internal electric field, $\xi_{int}(x)$, that will add to the externally applied electric field ξ_{ext}. Both the externally applied electric field and the internally developed space charge field will contribute to the current density under coherent illumination, which is given by

$$J_{coh} = \frac{1}{\Lambda}\int_0^{\Lambda}\left[q\mu_n n(x) + q\mu_p p(x)\right]\left[\xi_{ext} + \xi_{int}(x)\right]dx = J_0 + \Delta J(\Lambda) \quad , \tag{4.12}$$

where J_0 is the current density flowing under uniform illumination $I_0 = I_1 + I_2$. The sign of $\Delta J(\Lambda)$ is always negative, meaning that the current density flowing under coherent illumination is always less than that flowing under uniform illumination.

From the solution of Eqs. (4.3), (4.4) and (4.5), analytical expressions for $n(x)$, $p(x)$, and $\xi_{int}(x)$ can be obtained. Inserting them into Eq. (4.12), $\Delta J(\Lambda)$ can be obtained and the coefficient β can be calculated as

$$\beta = 1 + \frac{\Delta J(\Lambda)}{J_0 - J_1} \quad , \qquad (4.13)$$

where J_1 is the current density due to beam 1 alone. The analytical expression of $\Delta J(\Lambda)$ is rather complex, but in the high-Λ limit ΔJ (and therefore β, see Fig. 4.3a) tends towards a constant value. It has been shown [24] that, for undoped a-Si:H, in which electrons are the majority carriers, with a low external electric field and in the lifetime regime, this value is related to the density of states at the quasi Fermi level for trapped electrons, $N(E_{tn})$. The expression is

$$\Delta J(\Lambda \to \infty) = -\frac{1}{2} J_0 \left(\frac{\Delta G}{G_0}\right)^2 \frac{1}{(1+X_n)^2} \quad , \qquad (4.14)$$

where $X_n = C_n \tau_n k_B T N(E_{tn})$, with C_n the capture coefficient for electrons, τ_n the free electron lifetime, k_B the Boltzmann´s constant, T the absolute temperature, and E_{tn} the quasi Fermi level for trapped electrons. Taking into account the γ coefficient defined by Eq. (4.9), the following expression can be obtained

$$\frac{N(E_{tn})C_n}{\mu_n} = \frac{qG_0}{k_B T \sigma} \left[\frac{\gamma_0}{(1+G_2/G_1)} \sqrt{\frac{2(1+\gamma G_2/G_1)}{\gamma(1-\beta_{lim})}} - 1 \right] \quad , \qquad (4.15)$$

where β_{lim} is the constant value towards which the $\beta(\Lambda)$ curve tends for high Λ, and σ is the photoconductivity linked to G_0. Equation (4.15) expresses the DOS at the quasi Fermi level of trapped electrons as a function of material parameters (C_n and μ_n) and experimental quantities that can be easily measured (temperature, generation rate, photoconductivity, γ, γ_0 and β_{lim}). Since the material is assumed to be n-type, the quasi Fermi level of trapped electrons E_{tn} can be approximated by that of the free electrons, E_{Fn}, and evaluated from the steady-state photoconductivity σ as

$$E_{tn} \cong E_{Fn} \cong E_C - k_B T \ln\left(\frac{q\,\mu_n N_C}{\sigma}\right) \quad . \qquad (4.16)$$

It can be varied either by changing the temperature or the generation rate, giving the basis for a DOS spectroscopy in the upper half of the band gap. The experiment can be performed at a single grating period Λ, provided it is in the high-Λ region where the $\beta(\Lambda)$ curve tends towards a constant value. Thus, the experimental set-up is simple.

In order to illustrate the reconstruction of the DOS from this technique, we performed a numerical simulation starting from a typical DOS for hydrogenated amorphous silicon (solid line in Fig. 4.5). Taking standard values for the material parameters, the set of equations (4.3)-(4.5) and (4.12) have been numerically solved to get the $\beta(\Lambda)$ curves. Then, Eqs. (4.15)-(4.16) were applied to reconstruct the DOS, changing E_{tn} from a variation of T (circles) and G_0 (diamonds). Figure 4.5 shows that the initially introduced DOS can be reconstructed with good accuracy.

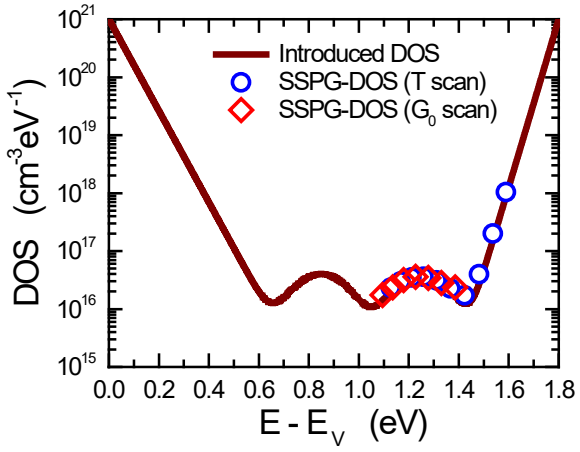

Figure 4.5. Test of the ability of Eqs. (4.15)-(4.16) to evaluate a typical DOS for a-Si:H. The quasi Fermi level has been shifted by changing the temperature and/or the generation rate.

In Eq. (4.15), the same quantity $N(E_{tn})\times C_n/\mu_n$ appears as for the DOS reconstruction from the MPC method performed in the high frequency regime (High frequency modulated photocurrent, HF-MPC) (see chapter 2). Thus, we compared the DOS reconstructions from both techniques on a standard a-Si:H sample. A He-Ne laser providing a generation rate $G_0 = 2\times10^{21}$ cm^{-3}s^{-1} has been used as a source of coherent illumination, with an intensity ratio $I_1/I_2 = 85$. The grating period was fixed at $\Lambda_{lim} = 10$ µm and the coefficients β and γ have been measured as a function of temperature, from 100 to 370 K in 30 K steps. Measurements have been performed under vacuum, at a pressure lower than 10^{-5} mBar. To obtain absolute DOS values an electron mobility $\mu_n = 10$ cm^{2}V^{-1}s^{-1} and a capture coefficient $C_n = 10^{-8}$ cm^{3}s^{-1} have been assumed in both methods. The results of the application of Eqs. (4.15)-(4.16) to the measured data are compared to the application of the HF-MPC DOS reconstruction, using the upper envelope of the MPC spectra as described in chapter 2 and displayed in Figure 4.6 (black full line). Note that energies are now referred to the conduction band edge, to avoid uncertainties in the value of the mobility gap for this sample. It can be appreciated that the agreement between the DOS determinations with both techniques is good over the energy range where they overlap.

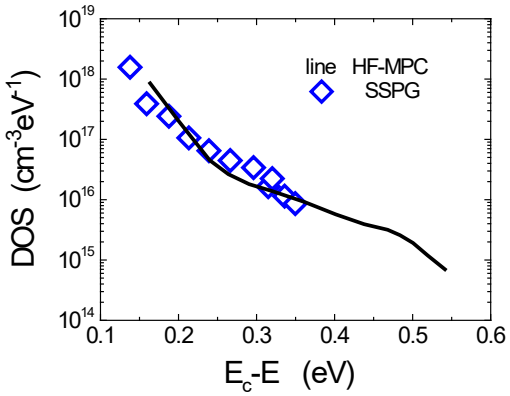

Figure 4.6. Comparison between DOS reconstructions from the modulated photocurrent technique in the high frequency regime (upper envelop of the HF-MPC spectra, black line) and from SSPG, both performed at several temperatures (diamonds).

The results above show that different techniques, here HF-MPC and SSPG, are complementary ones, and when applied to the same material they can lead to the same DOS spectroscopy. Moreover, it can be shown that, even with techniques that seem very different, the same expression for the DOS can be obtained. Indeed, assuming that $G_2 << G_1$, which is usually the case G_1 being at least 10 times larger than G_2, and which also means that $G_1 \approx G_0$, the theoretical calculation of β_{lim} leads to [25]

$$\beta_{\text{lim}} = 1 - 2\gamma\gamma_0^2 \quad . \qquad (4.17)$$

Replacing this expression into Eq. (4.15), and still assuming that $G_2 << G_1$, one obtains

$$\frac{N(E_{\mathrm{tn}})C_{\mathrm{n}}}{\mu_{\mathrm{n}}} = \frac{qG_0}{k_{\mathrm{B}}T\sigma}\left(\frac{1}{\gamma} - 1\right) \quad , \qquad (4.18)$$

which is exactly Eq. (2.26) presented in chapter 2 of this book, deduced from the theoretical developments on the possibility to achieve a DOS spectroscopy from the variations of the coefficient γ with temperature and/or generation rate.

4.3. Modulated photocarrier grating (MPG)

An extension of the 'classical' SSPG technique was proposed by K. Hattori and co-workers [2], and introduces a temporal component into this technique. Almost the same setup as the one proposed for SSPG is used, except that an electro-optic modulator (EOM) is installed on the probe beam path, EOM with which it is possible to modulate the polarization of the light. This experiment was called the modulated photocarrier grating (MPG) experiment. A schematic diagram of the bench developed by Hattori and co-workers is presented in Fig. 4.7. When the two beams have their polarizations parallel to the electrodes, an interference pattern is created, as in the case of SSPG and with the same spatial variation given by Eq. (4.7). The slow and fast axes of the EOM are set at 45° from the vertical and horizontal orientations of the light polarization, and, driving the EOM with a square wave at an angular frequency ω, the light polarization of the probe beam is modulated from vertical to horizontal. Therefore, the generation rate for MPG can be written as

$$G = G_0 + \Delta G_0 \cos(kx)\, S(t) \quad , \qquad (4.19)$$

where $S(t)$ is a square wave oscillating between 0 and 1 with an angular frequency ω. As a consequence, due to the alternating variation of the intensity of the interference pattern, the current flowing in between the electrodes is modulated at the same frequency and recorded via a lock-in amplifier after amplification by a current-voltage converter. To avoid a modification of the light reflection with the polarization of the probe beam, the latter is sent perpendicular to the film surface. As for the improved SSPG bench described in section 4.2.2, the expression of the grating spacing is thus slightly different from that of 'standard' SSPG with $\Lambda = \lambda/\sin(\theta)$, θ being the angle between the two beams.

Performing a Fourier series expansion of $S(t)$, and keeping only the terms that set the fundamental frequency of the modulated current, the generation rate can be written as

$$G = G_0 + \frac{\Delta G_0}{2}\cos(kx)\left(1 + \frac{4}{\pi}\cos(\omega t)\right) \quad . \qquad (4.20)$$

Note that this generation rate is close to the one originally proposed by K. Hattori and co-workers [2].

This technique was developed as a means to check for the conditions under which the interference pattern develops, and hence under which the photocurrent is measured: the lifetime regime or the dielectric relaxation time regime. Indeed, in the SSPG technique there is no possibility to distinguish between these two regimes, and therefore the estimate of the ambipolar diffusion length, which should be done in the lifetime regime, can be questionable.

Hattori and co-workers have given and solved the basic equations of the transport of electrons and holes in the MPG experiment, putting into evidence some key parameters that can be measured, and from the values of which it is possible to determine the regime of measurement as function of the experimental conditions. Applying this technique to the study of an a-Si:H sample, and combining the MPG experiment and the MPC experiment in the low frequency regime, they have shown that the

ambipolar diffusion length measured with the SSPG technique could be overestimated by a factor 2.5-3, the a-Si:H sample being not fully in the lifetime regime in the conditions of measurement.

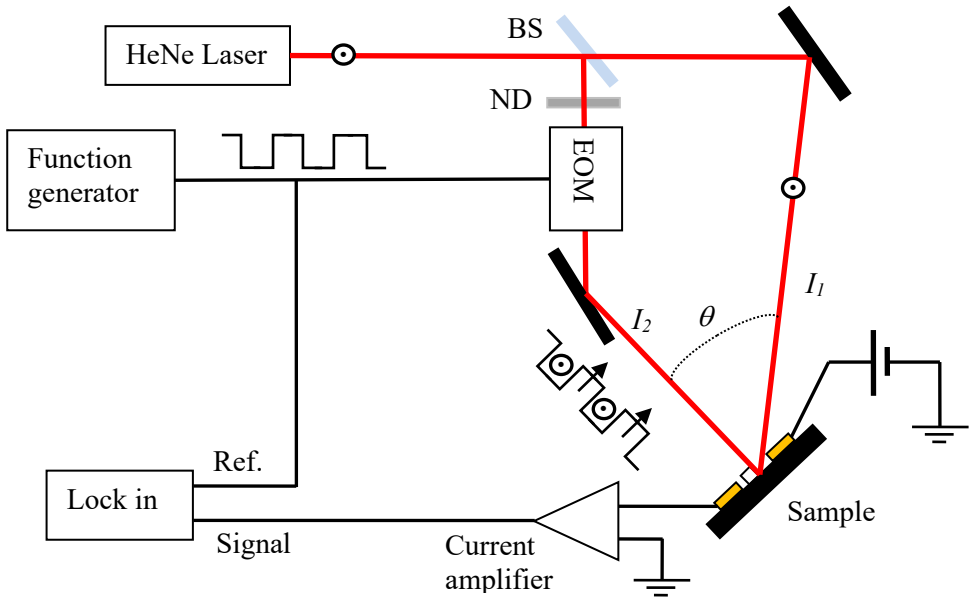

Figure 4.7. Schematic of the MPG set-up (from [2]).

However, in their theoretical analysis K. Hattori *et al.* defined phenomenological parameters, like the small signal trap-controlled mobilities and the recombination lifetimes, and worked with the total carrier concentrations (free plus trapped). On the other hand, J. A. Schmidt and co-workers [3] solved the fundamental MPG equations for the free carriers, using the multiple trapping model and the Simmons and Taylor's statistics for the recombination terms [26]. The simultaneous solution of the transport differential equations and of Poisson's equation allowed them to obtain the general solution of the problem starting from the DOS of the material, the capture coefficients and the extended states mobilities. Performing suitable approximations on the analytical solution of the MPG equations, Schmidt and co-workers obtained a simple formula relating the DOS at the electron quasi Fermi energy to material parameters and measurable quantities. The formula is valid for low electric fields (ξ_{ext} < 200 V/cm), high angular frequencies ($\omega \gg \tau_d^{-1}$), and high grating periods (Λ > 10 μm), with the additional assumption that electrons are the majority carriers and are more mobile than holes. Under these assumptions, the DOS at the quasi Fermi level for trapped electrons is given by

$$\frac{N(E_{tn})C_n}{\mu_n} = \frac{qG_0}{k_B T\sigma}\left[\frac{\sqrt{G_1 G_2}}{2G_0}\frac{|\Delta J_{MPC}|}{|\Delta J^{\omega}_{MPG}|} - 1\right] \quad , \qquad (4.21)$$

where $|\Delta J^{\omega}_{MPG}|$ is the modulus of the MPG signal at an angular frequency ω, and $|\Delta J_{MPC}|$ is the modulus of the MPC signal obtained under the same experimental conditions. As in the case of the DOS determination from SSPG, E_{tn} can be varied either by changing the temperature or the generation rate, giving the basis for a DOS spectroscopy in the upper half of the band gap. The experimental set-up is essentially the same for the MPG and MPC experiments, since the latter experiment only requires the introduction of a polarizer to prevent the beams from interfering. The advantage of Eq. (4.21) with respect to MPC alone is that only the modulus is needed, instead of both the modulus and the phase shift. This eliminates the additional need of calibrating for additional phase shifts introduced by the equipment used to measure the AC photocurrents.

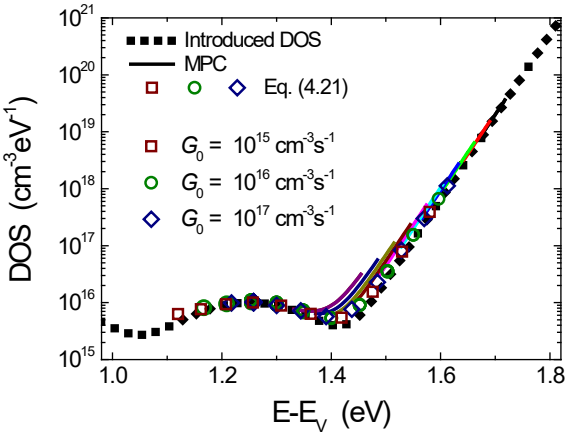

Figure 4.8. DOS used in our calculations (dotted line) and reconstructed from MPG by means of Eq. (4.21) (Symbols). The temperature was varied between 100 and 325 K in 25 K steps, for the generation rates indicated in the caption. For comparison the DOS reconstructed from HF-MPC using Eq. (2.55) is also shown (Full lines).

Starting from a typical DOS for hydrogenated amorphous silicon, Schmidt and co-workers performed a numerical simulation of the MPG and MPC experiments [3]. Standard values for the material parameters were taken (μ_n = 10 cm^{2}V^{-1}s^{-1}, μ_p = 1 cm^{2}V^{-1}s^{-1}, C_n = C_p = 10^{-8} cm^3/s), and the experimental conditions were chosen as a low electric field (ξ_{ext} = 100 V/cm), a high angular frequency (ω = 6×10^5 s^{-1}) and a high grating period (Λ = 20 μm). Then Eq. (4.21) was used to reconstruct the DOS, changing E_{tn} from a variation of T (100 K to 325 K in 25 K steps) and G_0 (10^{15} to 10^{17} cm^{-3}s^{-1}). Fig. 4.8 shows the reconstruction of the initially introduced DOS. As it can be seen, the DOS can be reconstructed with good accuracy. For comparison, the results of high-frequency MPC (see chapter 2) performed with the lowest generation rate are also presented.

4.4. Moving grating technique (MGT)

The moving grating technique (MGT) is also an extension of the 'classical' SSPG technique. It was developed by U. Haken, M. Hundhausen and L. Ley to introduce, as in the case of MPG, a temporal aspect which is missing in the standard SSPG [4, 5]. These authors have shown that it was possible to deduce independently the mobilities and lifetimes of holes and electrons from measurements of the short circuit current flowing in the film as function of the grating velocity v_{gr} and the grating period Λ.

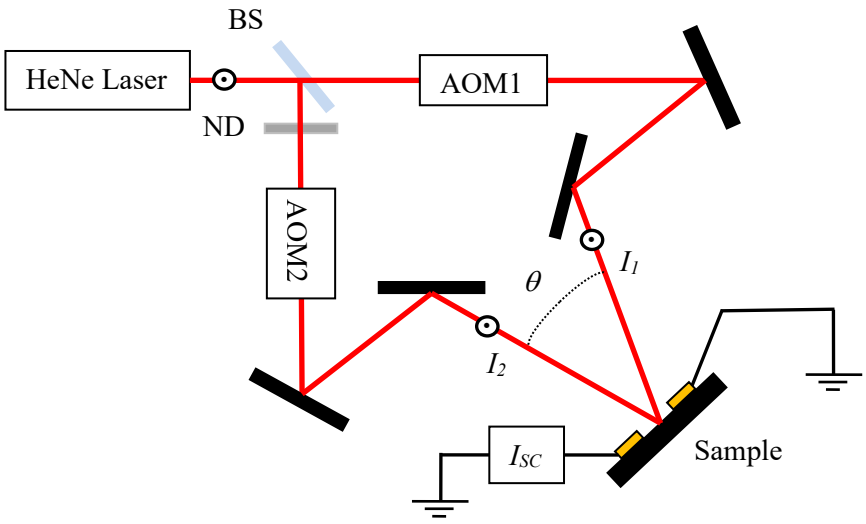

Figure 4.9. Schematic of the MGT setup (from [5]).

The experimental setup of the MGT is basically the same as for the SSPG and is presented in Fig. 4.9. A He-Ne laser beam, with polarization of the light parallel to the electrodes (perpendicular to the plane of the figure), is split in two beams by a beam splitter (BS). One of these beams is attenuated by a neutral density filter (ND), and then both beams are reflected by mirrors to illuminate the gap between the coplanar electrodes of the sample, making an angle θ between them ($\theta/2$ with the normal to the sample), to create interferences with a period Λ (See Eq. (4.6)). The major difference with SSPG is that acousto-optic modulators (AOMs) are inserted in the paths of the two beams used to generate interferences on the sample. The role of the AOMs is to shift the frequency of the light by $\Delta\nu_1$ and $\Delta\nu_2$, respectively, resulting in a frequency shift $\Delta\nu = \Delta\nu_1 - \Delta\nu_2$ between the two beams. This frequency shift causes a movement of the grating, in the plane of the film and along an axis perpendicular to the electrodes, with a velocity $v_{gr} = \Lambda\Delta\nu$. The intensity of the light illuminating the sample on an axis perpendicular to the electrodes at a position x from a reference electrode can be written

$$I(x,t) = I_1 + I_2 + 2\gamma_0\sqrt{I_1 I_2}\cos\left(\frac{2\pi}{\Lambda}\left(x - v_{\mathrm{gr}}t\right)\right) \quad , \qquad (4.22)$$

that gives a generation rate

$$G(x,t) = G_0 + \Delta G(x,t) = G_0 + g\cos\left[k\left(x - v_{\mathrm{gr}}t\right)\right] \quad . \qquad (4.23)$$

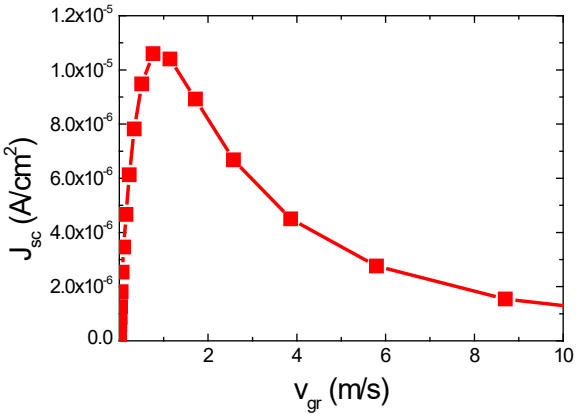

Figure 4.10. Variation of the photocurrent density with the grating velocity in an MGT calculation based on a 'standard' a-Si:H DOS.

The experimental quantity that is measured is the DC short circuit current density J_{SC} flowing between the electrodes, generated by the movement of the interferences perpendicularly to the electrodes, as function of the grating velocity or of the angular frequency defined by $\omega_{gr} = 2\pi v_{gr}/\Lambda$. Note that no external electric field is applied to the sample, and the current simply arises because of the movement of the light grating.

Fig. 4.10 displays a $J_{sc}(v_{gr})$ curve calculated from a 'typical' density of states of a-Si:H to illustrate the expected behaviors of J_{sc}, obtained here assuming a grating period of 4 µm and a generation rate of 10^{20} $cm^{-3}s^{-1}$. At low speed the current is almost equal to zero and rises when the grating velocity increases. After reaching a maximum, linked to a typical time constant of the material, the current density decreases with increasing velocity.

Starting from the continuity and Poisson's equations, and dealing with the total (free + trapped) electron and hole concentrations, n_T and p_T, respectively, U. Haken *et al.* have derived an expression of the photocurrent density as function of v_{gr} that can be written [5]

$$J_{\mathrm{sc}}\left(k, v_{\mathrm{gr}}\right) = \frac{c_1 v_{\mathrm{gr}}}{c_2 + c_3 v_{\mathrm{gr}}^2 + c_4 v_{\mathrm{gr}}^4} \quad , \qquad (4.24)$$

where $k = 2\pi/\Lambda$ and c_1, c_2, c_3, c_4 are constants given by

$$\begin{cases} c_1 = \frac{q^2}{2\varepsilon\varepsilon_0}\left(\mu_{n_T} + \mu_{p_T}\right)(g\tau_R)^2 k^2 \left(D_{n_T} - D_{p_T}\right) \\ c_2 = \frac{1}{\tau_R^2}\left[\left(a + \frac{(b+1)^2}{4b} l^2\right)(1 + l^2)\right]^2 \\ c_3 = k^2\left(1 + a^2 + \frac{(b+1)^2 + 2a(b^2+1)}{2b} l^2 + \frac{(b+1)^2(b^2+1)}{4b^2} l^4\right) \\ c_4 = k^4 \tau_R^2 \end{cases}, \qquad (4.25)$$

with the following notations

$$\begin{cases} a = \frac{\tau_R}{\tau_d} \\ b = \frac{\mu_{n_T}}{\mu_{p_T}} \\ l = k\sqrt{D\tau_R} \\ D = \frac{2D_{n_T}D_{p_T}}{D_{n_T} + D_{p_T}} \end{cases}. \qquad (4.26)$$

D_{n_T} and D_{p_T} are effective diffusion coefficients, linked via Einstein equations to the drift mobilities μ_{n_T} and μ_{p_T}, which differ from the free carriers mobilities because they take the multiple trapping process into account, and τ_R is the total photocarrier (free + trapped) recombination lifetime.

Playing with the above parameters, U. Haken and coworkers were able to fit the variations of $J_{sc}(v_{gr})$ to deduce the values of the mobilities. The grating velocity corresponding to the maximum, v_{grmax}, could be attributed either to the total recombination lifetime, $v_{grmax} = 1/k\tau_R$, or to the dielectric relaxation time, $v_{grmax} = 1/k\tau_d$, depending on the regime under which the sample is responding, *i. e.* the lifetime regime or the relaxation regime, respectively.

The advantages of this technique are that it is possible to determine separately the lifetimes and the mobilities of the carriers, to eventually deduce their respective diffusion lengths. Besides, an estimate of the recombination lifetime being possible from steady state measurements under illumination, it is possible to check the regime under which the measurements are performed.

However, a contradiction appeared when the MGT experiment was performed as a function of the illumination time elapsed during the light-induced degradation (light-soaking) of an a-Si:H thin film. The lifetime, deduced from the position of the maximum of the J_{sc} versus v_{gr} curve, seemed to increase with the light-soaking time, in opposition with what was expected. That is why the theoretical treatment of the MGT data was largely improved by J. A. Schmidt [27] to properly take into account recombination of carriers via the amphoteric deep states generated by dangling bonds. This apparent contradiction was explained by means of numerical calculations taking into account all the possible recombination paths.

Finally, a drawback of the MGT is the low level of the DC signal to be measured, which can be masked by the noise at low temperatures or low light intensities. Recently, L. Koppio and co-workers [28] proposed an alternating current (AC) version of the MGT by chopping the probe beam in the standard configuration. The technique was called the Chopped Moving photocarrier Grating (CMG). In CMG, the AC signal can be measured with a lock-in amplifier to increase the signal-to-noise ratio compared to the standard DC technique. The authors proved, both experimentally and with numerical simulations, the equivalence between MGT and CMG for low chopping frequencies.

4.5. Oscillating photocarrier grating (OPG)

Another characterization technique based on photocarrier grating was proposed by F. Ventosinos and co-workers [6] to investigate the density of states of thin film semiconductors. In this technique, a periodic spatial oscillation of the interference pattern is achieved, hence the name of oscillating photocarrier grating (OPG) technique. The amplitude of the oscillation is usually equal to half the grating period, and the movement occurs with constant velocity in each direction. The influence of the oscillation amplitude has been analyzed in a recent publication by L. Kopprio and co-workers [29]. The set-up designed to achieve such a movement is presented in Fig. 4.11. It is very similar to the one used for the MPG technique described above (Fig. 4.7). The only difference is that the EOM is set in the probe beam path, the axes of the crystal being aligned vertically and horizontally with the axes of the light polarization. In this 'phase modulation' configuration, the polarization and amplitude of the beam are not modified, but the phase of the wave is altered as function of the signal applied to the EOM. If the driving signal is a triangular function varying at an angular frequency ω, it can be shown that an expression of the intensity impinging the sample can be written

$$I(x,t) = I_1 + I_2 + 2\gamma_0\sqrt{I_1 I_2}\cos\left(\frac{2\pi x}{\Lambda} \pm \omega t\right) \quad , \qquad (4.27)$$

where the plus sign is for one half of a period and the minus sign is for the other half, and Λ is the grating period, $\Lambda = \lambda/\sin(\theta)$, θ being the angle between the two beams.

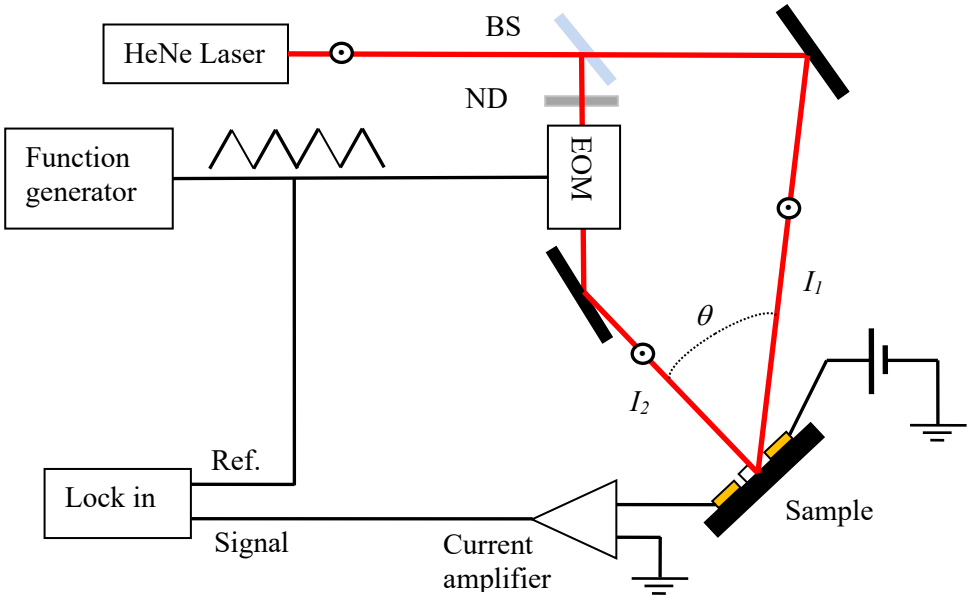

Figure 4.11. Schematic of the OPG set-up (from [6]).

As in the MGT technique, the displacement of the light grating between the electrodes results in the generation of a current even if no voltage bias is applied (short circuit conditions). However, in this case the signal is an alternating one and can be measured with a lock-in amplifier.

To illustrate this technique, and to show how it is linked to other techniques such as MGT, we present in Fig. 4.12 measurements of the excess photocurrents $\delta J(\omega)$ as function of the frequency of the light modulation, obtained on an a-Si:H sample with the OPG and MGT techniques under short circuit conditions. In the case of OPG the frequency was varied by playing with the modulation frequency of the EOM, whereas in the case of MGT, the frequency was varied by adjusting the difference between the excitation frequencies of the AOMs, resulting in a modification of the displacement velocity v_{gr} of the grating and, consequently, of the associated angular frequency ω_{gr}.

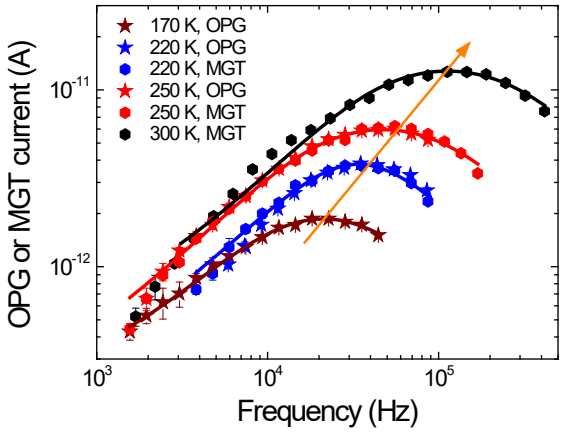

Figure 4.12. Variation of the OPG (stars) and MGT (circles) excess currents as function of the frequency at different temperatures, measured on an a-Si:H thin film. Full lines are fits obtained from Eq. (4.28).

It can be seen in Fig. 4.12 that the excess currents measured with both experiments are the same in the temperature range (220 – 250 K) where both techniques could be used. At low temperature (170 K) the excess current generated by MGT was too low to be detected accurately with an electrometer, whereas the use of a lock-in amplifier allows to improve the signal to noise ratio and to measure the excess of current in the OPG technique. At high temperature, the excess of current can be easily measured with an electrometer in the MGT experiment, whereas the limited bandwidth of the lock-in amplifier prevents measurements of the excess current in the OPG experiment in the high frequency range. These results show that these two techniques are complementary, because the use of both techniques extends the ranges of frequency and temperature that can be explored. The same type of experiment can also be performed at a fixed temperature with different fluxes of light, and the same type of behavior is observed. At low generation rates OPG is best suited because of its better sensitivity, at intermediate generation rates both techniques, MGT and OPG, give the same results, and at high generation rates the MGT is more appropriate because of the bandwidth limitation of the apparatus used to record the OPG excess current.

Fig. 4.12 also shows that the excess currents present a clear maximum that can be explained the following way. The light grating impinging on the sample creates several arrays, in particular an array of free carriers $n(x)$ and an array of trapped carriers $N_{trap}(x)$. With a large Λ, $N_{trap}(x)$ does not vanish by diffusion and eventually creates a space charge array that results in an internal electric field array $\xi_{int}(x)$. With a static grating, as in the SSPG technique, $n(x)$ and $\xi_{int}(x)$ are in quadrature, implying that the excess of current is null without an external electric field (Eq. (4.12)). When the light array is moving along the film surface with a relatively low velocity, the free carriers grating follows it almost instantaneously, whereas the space charge array lies behind due to the necessary delay the trapped carriers need to reorganize. The $n(x)$ and $\xi_{int}(x)$ arrays are no longer in quadrature and a current may appear from the movement of free carriers (mostly electrons in a-Si:H) in the internal field, a current that exists even though the external field is zero. With a low external electric field applied, the alternating current is still mainly due to the internal field and we have obtained the same variations of $\delta J(\omega)$ as with zero field applied [6].

As ω increases the velocity of the light grating increases too, and the phase lag between $n(x)$ and $\xi_{int}(x)$ tends to decrease, resulting in a steady increase of the OPG or MGT currents. However, if the time needed for the light to cover a distance Λ becomes too small, the trapped charges do not have time to reorganize and to follow the light array. The space charge array starts to blur, and the result is a decrease of the local internal field. The competition between the decrease of the phase shift between $n(x)$ and $\xi_{int}(x)$, and the blurring of the space charge, eventually yields a decrease of the OPG or MGT current density with increasing ω.

One can try to link the frequency of the maximum of the curves to a characteristic time of the material. Three times can be considered: the dielectric relaxation time τ_d, the lifetime of the free majority carriers, in the case of a-Si:H that of the electrons, τ_n, and the small signal recombination lifetime τ'_n that is the lifetime of the excess of free plus trapped electrons. Numerical simulations have been used to find out which of these three time constants could correspond to the position of the maximum of $\delta J(\omega)$. In these calculations we have introduced a standard a-Si:H DOS made of two band tails and deep defects represented by two Gaussian distributions, and reproduced all the experimental behaviors as function of temperature and generation rate.

In Fig. 4.13 are presented the evolutions of the different characteristic times and of the reciprocal of ω_{max} as functions of the generation rate. It can be seen that at low generation rates the position of the maximum of $\delta J(\omega)$ is linked to the dielectric relaxation time, whereas at high generation rates this position is linked to the small signal recombination lifetime. Information on the DOS can thus be extracted from the OPG and/or MGT data, provided an accurate value of ω_{max} can be extracted from the $\delta J(\omega)$ curve. However, it can be seen in Fig. 4.12 that if one considers the measured data points the determination of the maximum position is far from being very precise.

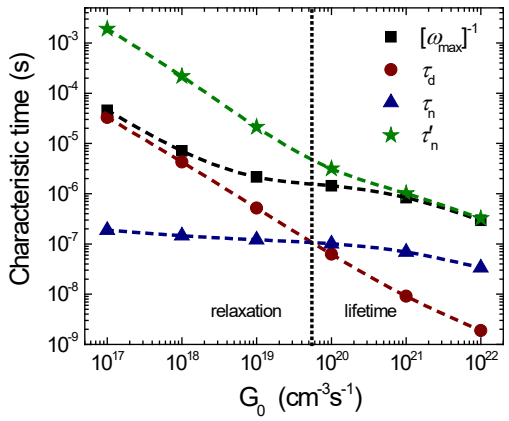

Figure 4.13. Results from a numerical simulation showing the evolution of the different characteristic times as well as that of $1/\omega_{max}$ as function of the generation rate G_0. Dashed lines are guides to the eye. The transition from the relaxation to the lifetime regime is shown by a vertical dotted line.

A complete theoretical calculation of $\delta J(\omega)$ for the OPG experiment, that it would be too long to reproduce here, has been performed in [30]. The result obtained shows that, in the case where $\omega\tau_d$ is much smaller than one, this expression is equivalent to a second order band pass filter. Hence, one can use a classical expression of this type of filter to fit the curves displayed in Fig. 4.12

$$\delta J(\omega) = \frac{\delta J_{max}}{\sqrt{1+Q^2\left[\frac{\omega_{max}}{\omega}-\frac{\omega}{\omega_{max}}\right]^2}} \quad , \qquad (4.28)$$

where δJ_{max}, ω_{max}, and Q correspond respectively to the maximum value of the current, the angular frequency of this maximum, and a 'quality factor' of the band pass filter. The excellent agreement between the experimental data points and the fitting curves can be seen in Fig. 4.12. The reader must note that this fit is only phenomenological and can be considered as a guide, or a help, to determine more accurately the δJ_{max} and ω_{max} values from the data points of the $\delta J(\omega)$ curve. It must be noted also that this type of fit is only valid in the case where $\omega\tau_d$ is much smaller than one, i.e., in the lifetime regime, otherwise the order of the band pass filter would be higher and the fit would not be as good as it is in Fig. 4.12. Hence, in addition to the improvement of the accuracy for determining the δJ_{max} and ω_{max} values, this phenomenological fit has also the advantage to put rapidly into evidence that the experiments are really performed in the lifetime regime. In this regime one can estimate the

small signal recombination lifetime, from which a DOS spectroscopy can be achieved, as shown in the following section.

4.6. DOS determination from the small signal recombination lifetime.

The knowledge of the small signal recombination lifetime τ_n', obtained either from MGT or OPG, is very interesting because this time is linked to the trapped carriers. Therefore, it is expected that information about the DOS can be gained from it. A definition of τ_n' was given by Y. M. Li [14]

$$\tau_n' = \frac{\partial N^-}{\partial G_0} = \frac{\partial [n + \int f(E)\, N^{ACC}(E)\, dE]}{\partial G_0} \quad , \qquad (4.29)$$

where N^- is the total concentration of negatively charged species linked to the free (n) plus trapped electron concentrations, $f(E)$ the probability for a state at energy E being occupied by an electron and $N^{ACC}(E)$ the density of acceptor states (negatively charged when occupied). As shown by Ventosinos and co-workers [6], a first-order approximation of the integral in Eq. (4.29) leads to

$$\tau_n' \cong \frac{\gamma}{G_0}\left[n + k_B T N^{ACC}(E_{Fn})\right] \quad , \qquad (4.30)$$

where E_{Fn} is the free electrons quasi Fermi level, given by

$$E_C - E_{Fn} = k_B T \ln\left[q\mu_n N_C / \sigma\right] \quad . \qquad (4.31)$$

As usually done in disordered semiconductors, where the density of trapped carriers is much larger than the density of free carriers, we can neglect n in Eq. (4.30), obtaining

$$N^{ACC}(E_{Fn}) \cong \frac{G_0 \tau_n'}{\gamma k_B T} \quad . \qquad (4.32)$$

Equation (4.32), coupled with Eq. (4.31), allows for a DOS spectroscopy if the experiment is performed at different temperatures.

Using a numerical simulation, in which a typical a-Si:H DOS was introduced (see Figure 4.1), calculations of τ_n' and γ were performed by Longeaud and co-workers [30] for temperatures ranging from 100 to 460 K with a generation rate G_0=10^{21} cm^{-3}s^{-1}. A characteristic temperature of 300 K was used for the CBT. The capture coefficients of the CBT and deep states were chosen identical and equal to C_n = 10^{-8} cm^{3}s^{-1}. The DOS spectroscopy based on the simplified Eq. (4.32) is displayed in Fig. 4.14 (circles), where the general trends of the original DOS, displayed by a full line, are well reproduced but the precision is rather poor.

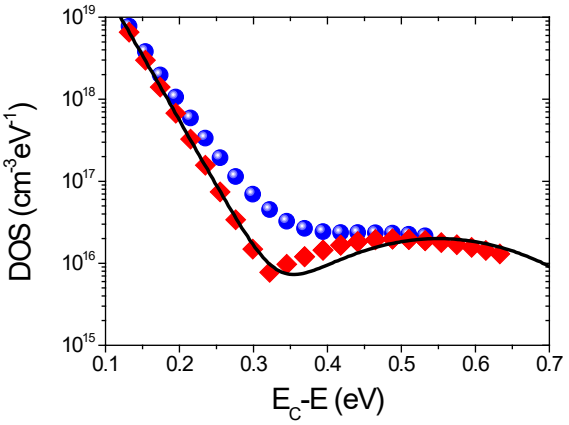

Figure 4.14. DOS spectroscopy from the OPG or MGT techniques with a simple procedure (circles) or after correction (diamonds). The full line displays the original DOS.

For materials such as a-Si:H, in which the band tails are assumed to decrease exponentially with energy, the τ'-DOS spectroscopy of the conduction band tail states can be refined calculating more accurately the integral of Eq. (4.29). Such a calculation has been performed by Longeaud and co-workers [30], obtaining the expression

$$N^{\mathrm{CBT}}(E_{\mathrm{Fn}}) = \frac{G_0 \tau_{\mathrm{n}}'}{\gamma k_{\mathrm{B}} T} \frac{\alpha\pi}{\sin(\alpha\pi)} \quad , \qquad (4.33)$$

where $\alpha = {}^{T}/_{T_{\mathrm{C}}}$, T_{C} being the characteristic temperature of the conduction band tail. Equation (4.33) is valid only for $T < T_C$, and it is a recursive expression, since T_{C} is needed to obtain N^{CBT}. Thus, a first approximation can be obtained from Eq. (4.32), which can be corrected by Eq. (4.33). Following this procedure, Longeaud and co-workers find the τ'-DOS displayed as diamonds in Fig. 4.14, for which the agreement with the introduced DOS is excellent.

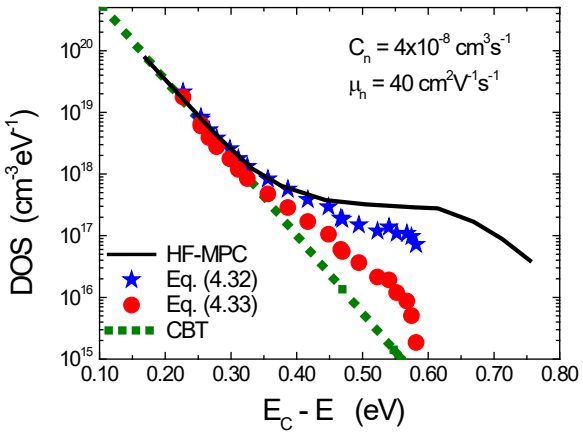

Figure 4.15. DOS spectroscopies achieved with the HF-MPC technique (black line) and the OPG/MGT techniques (symbols). Both equations (4.32) and (4.33) have been used to plot the OPG/MGT results. The dotted line represents the exponentially decreasing conduction band tail (CBT) extrapolated from the spectroscopies.

To check if these theoretical developments were experimentally applicable, we have carried out some complementary experiments on several a-Si:H samples and, in particular, on the sample with which we have obtained the results presented in Fig. 4.12. Since the OPG and MGT techniques have to be performed with large fluxes, the samples were light-soaked before measurement to avoid a possible evolution of the DOS during the experiments. These two techniques were performed with a He-Ne laser, the flux of the main beam being equal to 1.5×10^{17} cm^{-2}s^{-1}, the probe beam being attenuated by a factor of 20, and the grating period being equal to Λ = 5 μm. The temperature was varied in the range 110 K- 390 K, each 10 K below 250 K and each 20 K above. For each temperature we have calculated the γ coefficient from SSPC measurements. On the same sample we have performed MPC experiments with a red light (650 nm), a DC flux of 10^{14} cm^{-2}s^{-1}, an AC flux three times lower, each 20 K in the same range of temperatures. All the details on the sample preparation and experiments applied to that sample can be found in [30]. In Fig. 4.15 we present the DOS spectroscopies deduced from the results of these experiments. The OPG/MGT DOS was calculated either with Eq. (4.32) or Eq. (4.33), this last expression being valid only when probing the CBT. It is also worth to recall that the MPC spectroscopy gives only access to the variations of the quantity $N(E)C_{\mathrm{n}}/\mu_{\mathrm{n}}$ whereas the OPG/MGT spectroscopy gives access to the $N(E)$ variations. Hence, assuming an equivalent density of states $N_{\mathrm{C}} = 2.5\times10^{19}$ cm^{-3} at the bottom of the conduction band, we had to adjust the capture coefficient and the extended states mobility to $C_{\mathrm{n}} = 4\times10^{-8}$ cm^{3}s^{-1} and $\mu_{\mathrm{n}} = 40$ cm^{2}V^{-1}s^{-1}, respectively, to reach a match in the CBT region of the deduced DOS and of the energy scaling for all the techniques. With these values it can be seen that an excellent agreement is found between the DOS deduced from the different techniques and/or equations in the range 0.21 – 0.32 eV in the CBT region. Concerning the deeper states, there is a clear disagreement between the HF-MPC-DOS and the OPG-DOS calculated from Eq. (4.33), which is not surprising since the latter expression is

valid only in the CBT region where the DOS is exponentially decreasing with energy. On the other hand, the discrepancy between the MPC-DOS and the OPG-DOS deduced from the more general Eq. (4.32) may come from the fact that the deep states capture coefficient is not equal to the CBT capture coefficient. According to Fig. 4.15, the ratio between these two coefficients would be of the order of 3.

These results show that, by combining different characterisation techniques, it is possible to deduce both a DOS spectroscopy and some of the transport parameters for the material under study.

A further refinement of Eq. (4.33) has been proposed by L. Kopprio and co-workers [31], applicable to the conduction band tail of amorphous photoconductors

$$N^{\mathrm{CBT}}(E_{\mathrm{tn}}) \cong \frac{q\,\mu_{\mathrm{n}} \sin\left(\frac{\pi T}{T_{\mathrm{C}}}\right)\left(\frac{R_{\mathrm{C}}\sigma}{q\mu_{\mathrm{n}}}+\frac{G_0 L_{\mathrm{amb}}^2}{2k_{\mathrm{B}}T\mu_{\mathrm{p}}}\right)^2\left(\tau'-\frac{\gamma\sigma}{q\,\mu_{\mathrm{n}}G_0}\right)}{R_{\mathrm{C}}\,\pi\,\sigma\left(\gamma\left(\frac{L_{\mathrm{amb}}^2}{2\mu_{\mathrm{p}}}+\frac{R_{\mathrm{C}}\,\sigma\,k_{\mathrm{B}}T^2}{q\mu_{\mathrm{n}}G_0\,T_{\mathrm{C}}}\right)-\frac{L_{\mathrm{amb}}^2}{\mu_{\mathrm{p}}}\left(\frac{1}{2}+\gamma_{\mathrm{L}}\right)\left(1-\frac{T}{T_{\mathrm{C}}}\right)\right)} \quad , \tag{4.34}$$

$$E_{\mathrm{tn}} \cong E_{\mathrm{C}} + k_{\mathrm{B}}T \ln\left(\frac{\frac{R_{\mathrm{C}}\sigma}{q\mu_{\mathrm{n}}}+\frac{G_0 L_{\mathrm{amb}}^2}{2k_{\mathrm{B}}T\mu_{\mathrm{p}}}}{R_{\mathrm{C}}\,N_{\mathrm{C}}}\right) \quad , \tag{4.35}$$

where $R_{\mathrm{C}} = \frac{C_{\mathrm{n}}^{\mathrm{CBT}}}{C_{\mathrm{p}}^{\mathrm{CBT}}}$ is the ratio of the capture coefficients for electrons and holes in the conduction band tail, and L_{amb} is the ambipolar diffusion length that can be measured with the SSPG technique (see Section 4.2.1). In Eq. (4.34) also appears the exponent γ_{L} of the logarithmic derivative of the ambipolar diffusion length with respect to the steady and uniform generation rate G_0,

$$\gamma_{\mathrm{L}} = \frac{\partial \ln(L_{\mathrm{amb}})}{\partial \ln(\mathrm{G}_0)} \quad . \tag{4.36}$$

Therefore, to use Eqs. (4.34) and (4.35), measurements of the photoconductivity σ and L_{amb} as a function of G_0 are needed, as well as estimates of R_{C} and the extended-states mobilities μ_{n} and μ_{p}.

For a semiconductor under steady state conditions, the total concentration of electrons (free + trapped) n_{T} should be equal to the total concentration of holes p_{T}, as required by charge neutrality. Consequently, the partial derivatives with respect to the generation rate should also be equal: $\tau_{\mathrm{n}}' = \partial n_{\mathrm{T}}/\partial G_0$ should be equal to the corresponding time for holes, $\tau_{\mathrm{p}}' = \partial p_{\mathrm{T}}/\partial G_0$. Therefore, this common small-signal recombination lifetime τ' should provide information not only about the CBT but also about the valence band tail (VBT), as has been shown by L. Kopprio *et al.* [31]

$$N^{\mathrm{VBT}}\left(E_{\mathrm{tp}}\right) \cong \frac{2\mu_{\mathrm{p}} \sin\left(\frac{\pi T}{T_{\mathrm{V}}}\right)\left(\frac{R_{\mathrm{V}}\,\sigma}{q\,\mu_{\mathrm{n}}}+\frac{G\,L_{\mathrm{amb}}^2}{2\mu_{\mathrm{p}}k_{\mathrm{B}}T}\right)^2\left(\tau'-\left(\frac{1}{2}+\gamma_{\mathrm{L}}\right)\frac{L_{\mathrm{amb}}^2}{k_{\mathrm{B}}T\mu_{\mathrm{p}}}\right)}{\pi\,L_{\mathrm{amb}}^2\left(\frac{R_{\mathrm{V}}\,\gamma\,\sigma}{q\,\mu_{\mathrm{n}}}\left(\frac{T}{T_{\mathrm{V}}}-1\right)+(1+2\gamma_{\mathrm{L}})\left(\frac{R_{\mathrm{V}}\,\sigma}{q\,\mu_{\mathrm{n}}}+\frac{G\,L_{\mathrm{amb}}^2}{2\mu_{\mathrm{p}}k_{\mathrm{B}}T_{\mathrm{V}}}\right)\right)} \quad , \tag{4.37}$$

$$E_{\mathrm{tp}} \cong E_{\mathrm{V}} - k_{\mathrm{B}}T \ln\left(\frac{\frac{R_{\mathrm{V}}\,\sigma}{q\,\mu_{\mathrm{n}}}+\frac{G\,L_{\mathrm{amb}}^2}{2\mu_{\mathrm{p}}k_{\mathrm{B}}T}}{N_{\mathrm{V}}}\right) \quad , \tag{4.38}$$

where E_{V} is the energy of the valence band edge, $R_{\mathrm{V}} = \frac{C_{\mathrm{n}}^{\mathrm{VBT}}}{C_{\mathrm{p}}^{\mathrm{VBT}}}$ is the ratio of the capture coefficients for electrons and holes in the valence band tail, E_{tp} is the quasi Fermi level for trapped holes, T_{V} is the characteristic temperature of the valence band tail, and N_{V} is the effective density of states at the valence band edge. With the exception of N_{V} and R_{V}, Eqs. (4.37) and (4.38) include the same parameters as Eqs. (4.34) and (4.35), therefore, if the parameters have been measured to obtain one of

the band tails, it should be possible to get the other band tail without performing almost any additional measurement.

4.7. Conclusions

In this chapter, we have described four characterisation techniques based on the illumination of the studied sample with an interference pattern and measurement of the resulting photocurrent. In one experiment, the steady-state photocarrier grating (SSPG) technique, the pattern is static and the current is measured as a function of the grating spatial period at low applied voltage bias. Since the ambipolar diffusion influences the development of a space charge grating under the light generation, the ambipolar diffusion length can be determined by playing with the grating period. The method proved to be very fruitful for the characterization of amorphous and defective photoconductors. An automated setup for the implementation of the SSPG experiment has been proposed, which saves time and improves the accuracy of the measurement. Also, a procedure has been proposed to extract part of the DOS within the bandgap of the studied semiconductor based on SSPG measurements.

There are several ways to introduce the temporal aspect in the SSPG experiment. One possibility is the modulated photocarrier grating (MPG) technique, which consists in changing from a condition with interferences to a condition of uniform illumination with a certain frequency. The resulting photocurrent is measured in AC as a function of frequency. The method has been originally used for testing the ambipolarity condition as well as for measuring the diffusion length of both carriers. More recently, a procedure to extract part of the DOS from MPG measurements has been proposed.

The moving grating technique (MGT) is another way of introducing the temporal aspect in the SSPG experiment. In this case, the grating moves at a constant velocity in one direction, resulting in a DC current even with no applied voltage bias. A measurement as a function of the grating velocity provides information on the carriers' drift mobilities and the common recombination lifetime.

In the oscillating photocarrier grating (OPG) technique, the pattern oscillates with a certain frequency, moving with constant velocity in one direction during half a period and in the other direction during the other half. The OPG technique can then be considered as an AC version of the MGT, and it has been shown that both techniques give the same results when the conditions of applicability are fulfilled. With a proper treatment of the OPG/MGT data, performing these experiments at different temperatures, a density of states spectroscopy can be achieved. Three possible treatments have been proposed, a general one that can be applied to probe any distribution of states, and two more refined treatments, with different degrees of sophistication, that are well suited for exponentially decreasing band tails.

In summary, photocarrier grating techniques provide valuable information on the transport parameters and the density of states of defective photoconductors.

Appendix: Notations used for the most important quantities (by alphabetic order)

C_n	Capture coefficient of a trap for electrons of the conduction band	(cm^3s^{-1})
C_p	Capture coefficient of a trap for holes of the valence band	(cm^3s^{-1})
D_n	Diffusion coefficient for electrons	(cm^2s^{-1})
D_p	Diffusion coefficient for holes	(cm^2s^{-1})
E	Energy of a state	(eV)
E_C	Energy of the bottom of the conduction band	(eV)
E_{Fn}	Quasi Fermi level for free electrons	(eV)
E_{tn}	Quasi Fermi level for trapped electrons	(eV)
E_{tp}	Quasi Fermi level for trapped holes	(eV)
E_V	Energy of the top of the valence band	(eV)

$f(E)$	Occupation function of a monovalent state at the energy E under light	
G	Generation rate	($cm^{-3}s^{-1}$)
G_0	Generation rate due to the sum of the main and probe beams (uniform and steady)	($cm^{-3}s^{-1}$)
G_1	Generation rate due to the main beam	($cm^{-3}s^{-1}$)
G_2	Generation rate due to the probe beam	($cm^{-3}s^{-1}$)
$I(x)$	Intensity of the light impinging the sample at x	($cm^{-2}s^{-1}$)
I_1	Intensity of the light of the main beam	($cm^{-2}s^{-1}$)
I_2	Intensity of the light of the probe beam	($cm^{-2}s^{-1}$)
I_{wi}	Current measured with interferences	(A)
I_{woi}	Current measured without interferences	(A)
J_0	Density of current measured under uniform illumination	(Acm^{-2})
J_1	Density of current due to the main beam alone	(Acm^{-2})
J_{coh}	Density of current measured under coherent illumination	(Acm^{-2})
J_n	Electron current density	(Acm^{-2})
J_p	Hole current density	(Acm^{-2})
J_{SC}	Current density measured under short circuit conditions	(Acm^{-2})
k	wave number ($2\pi/\lambda$)	(cm^{-1})
k_B	Boltzmann's constant	(8.617×10^{-5} eVK^{-1})
L_{amb}	Ambipolar diffusion length	(cm)
n	Free electron concentration under light	(cm^{-3})
n_T	Total concentration of electrons (free+trapped)	(cm^{-3})
$N(E)$	Density of states at the energy E	($cm^{-3}eV^{-1}$)
$N^{ACC}(E)$	Density of acceptor states at E	($cm^{-3}eV^{-1}$)
$N^{DON}(E)$	Density of donor states at E	($cm^{-3}eV^{-1}$)
N_C	Equivalent density of states at the bottom of the conduction band	(cm^{-3})
N_V	Equivalent density of states at the top of the valence band	(cm^{-3})
p	Free hole concentration under light	(cm^{-3})
p_T	Total concentration of holes (free + trapped)	(cm^{-3})
q	Absolute value of the electronic charge	(1.6×10^{-19} C)
R_n	Recombination rate for electrons	($cm^{-3}s^{-1}$)
R_p	Recombination rate for holes	($cm^{-3}s^{-1}$)
t	Time	(s)
T	Temperature of the material	(K)
T_C	Characteristic temperature of the exponential conduction band tail	(K)
T_V	Characteristic temperature of the exponential valence band tail	(K)
v_{gr}	Grating velocity	(cm s^{-1})
x	Distance	(cm)

α	T/T_C	
β	Ratio of the current with interferences to the current without interferences	
γ	Coefficient defined by the logarithmic derivative of σ with respect to G	
γ_L	Coefficient defined by the logarithmic derivative of L_{amb} with respect to G_0	
γ_0	Coefficient defining the interference quality ($0\leq \gamma_0 \leq 1$)	
$\Delta\nu$	Difference of the frequencies of light of the two beams	(Hz)
ε	Dielectric constant of the material	

ε_0	Vacuum permittivity	(8.854×10^{-14} Fcm^{-1})
θ	Angle between the two light beams	(radian)
λ	Wavelength of the light	(μm)
Λ	Grating period	(μm)
ν	Frequency of the light	(Hz)
μ_n	Extended states electron mobility	($cm^2V^{-1}s^{-1}$)
μ_p	Extended states hole mobility	($cm^2V^{-1}s^{-1}$)
ξ	Electric field	(Vcm^{-1})
ξ_{ext}	Externally applied electric field	(Vcm^{-1})
ξ_{int}	Internal electric field	(Vcm^{-1})
σ	Photoconductivity of the material	(Scm^{-1})
τ_d	Dielectric relaxation time	(s)
τ_n	Free electron lifetime	(s)
τ'_n	Small signal recombination lifetime of the excess of free + trapped electrons	(s)
τ_p	Free hole lifetime	(s)
τ'_p	Small signal recombination lifetime of the excess of free + trapped holes	(s)
τ_R	Overall recombination lifetime of the carriers (free + trapped)	(s)
ω	Angular frequency of the modulation of the light	(s^{-1})

Acknowledgements

Many thanks to Pere Roca i Cabarrocas, from the Laboratoire de Physique des Interfaces et Couches Minces (LPICM, Palaiseau, France) for the deposition of a-Si:H and pm-Si:H films and devices, and to Michel Police and Richard Andlauer for technical assistance

We thank the SOLSIA company for providing some of the a-Si:H samples in the framework of the POLYSIL project funded by the Agence de l'Environnement et de la Maîtrise de l'Energie (ADEME)

Part of this work was made under Ecos-Sud projects A02E01, A08E01, and A13E02.

J. S. thanks the "Make Our Planet Great Again" Short-Stay program.

References

1 Ritter, D., Zeldov, E., Weiser, K. (1986). *Appl. Phys. Lett.* 49: 791.
2 Hattori, K., Koji, Y., Fukuda, S., Ma, W., Okamoto, H. (1993). *J. Appl. Phys.* 73: 3846.
3 Schmidt, J. A., Budini, N., Ventosinos, F., Longeaud, C. (2010) *Phys. Status Solidi A* 207: 556-560.
4 Haken, U., Hundhausen, M., Ley, L. (1993) *Appl. Phys. Lett.* 63: 3066.
5 Haken, U., Hundhausen, M., Ley, L. (1995) *Phys. Rev. B* 51: 10579.
6 Ventosinos, F., Budini, N., Longeaud, C., Schmidt, J. A. (2011) *J. Phys. D: Appl. Phys.* 44: 295103.
7 Stepanov, S. (2001) in Handbook of Electronic and Photonic Materials and Devices (Vol. 2), Edited by H. S. Nalwa, (Academic Press) : 205.
8 Ritter, D., Weiser, K., Zeldov, E. (1987) *J. Appl. Phys.* 62: 4563.
9 Balberg, I., Delahoy, A. E., Weakliem, H. A. (1988) *Appl. Phys. Lett*. 53: 992.
10 Sauvain, E., Chen, J. H. (1994) *J. Appl. Phys.* 75: 5191.
11 Abel, C. -D., Bauer, G. H., Bloss, W. H. (1995) *Philos. Mag. B* 72: 551.
12 Balberg, I. (1991) *Phys. Rev. B* 44: 1628.
13 Balberg, I. (1990) *J. Appl. Phys.* 67: 6329.
14 Li, Y. M. (1990) *Phys. Rev. B* 42: 9025.
15 Hattori, K., Okamoto, H., Hamakawa, Y. (1992) *Phys. Rev. B* 45: 1126.
16 Haridim, M., Zelikson, M., Weiser, K. (1994) *Phys. Rev. B* 49: 13394.

17 Sauvain, E., Hubin, J., Shah, A., Pipoz, P. (1991) *Philos. Mag. Lett.* 63: 327.
18 Haridim, M., Weiser, K., Mell, H. (1993) *Philos. Mag. B* 67: 171.
19 Brüggemann, R. (2010) *J. Phys.: Conference Series* 253(1): 012081.
20 Brüggemann, R. (2011) in *Advanced Characterization Techniques for Thin Film Solar Cells*, Second Edition, Edited by D. Abou-Ras,T. Kirchartz, U. Rau, (Wiley-VCH Verlag) p. 163.
21 Longeaud, C., Fath Allah, A., Schmidt, J. A., El Yaakoubi, M., Berson, S., Lemaitre, N. (2016) *Organic Electronics* 31: 253-257.
22 Longeaud, C. (2013) *Rev. Sci. Instrum.* 84: 055101.
23 Longeaud, C., Ramos, F. J., Rebai, A., Rousset, J. (2018) *Sol. RRL*: 1800192.
24 Schmidt, J. A., Longeaud, C., (2005) *Phys. Rev. B* 71: 125208.
25 Longeaud, C., Schmidt, J. A., Kleider, J. P. (2006) *Phys. Rev. B* 73: 235316.
26 Simmons, J. G., Taylor, G. W. (1971) *Phys. Rev. B* 4: 502.
27 Schmidt, J. A., Hundhausen, M., Ley, L. (2001) *Phys. Rev. B* 64: 104201.
28 Kopprio, L., Ventosinos, F., Schmidt, J. A. (2019) *Rev. Sci. Instrum*. 90: 123902.
29 Kopprio, L., Longeaud, C., Ventosinos, F., Schmidt, J. A. (2021) *Applied Physics B* 127 (28).
30 Longeaud, C., Ventosinos, F., Schmidt, J. A. (2012) *J. Appl. Phys.* 112: 023709.
31 Kopprio, L., Longeaud, C., Schmidt, J. A. (2017) *J. Appl. Phys.* 122: 085702.